Available online at www.sciencedirect.com

ScienceDirect

Procedia CIRP 13 (2014) 294 – 301

www.elsevier.com/locate/procedia

2nd CIRP 2nd CIRP Conference on Surface Integrity (CSI)

Effect of constitutive modeling during finite element analysis of machining-induced residual stresses in Ti6Al4V

Gary Styger[a]*, Rudolph F Laubscher, Gert A Oosthuizen

[a]*University of Johannesburg, Corner Kingsway and University Road, Auckland Park 2006, South Africa*

* Corresponding author. Tel.: +27-73-230-8365; fax: +27-11-559-2532 *E-mail address*: garystyger@gmail.com

Abstract

Residual stress is an important surface integrity descriptor that may have a marked effect on the functional performance of machined alloy parts. This paper describes a finite element evaluation of the effect of different constitutive models on machining induced residual stresses for Ti6Al4V titanium alloy. A two dimensional orthogonal turning process is modelled and the results compared to experimental data. Residual stress is evaluated with respect to different elastic-viscoplastic constitutive models at certain cutting speeds and feeds. The general-purpose finite element code MSC Marc@ was used with comparisons with experimental data made relative to residual stress, cutting force and temperature. The magnitude and extent (depth) of the residual stress field is evaluated with regards to the different material models and compared with experimental data.

Keywords: Residual stress; Machining; Constitutive model

1. Introduction

Titanium alloys are utilised in the aeronautical, aerospace as well as medical industries largely because of its corrosion resistance and excellent strength to weight ratio. Ti6Al4V (Grade 5) is the most popular titanium alloy in mainstream use today.

The manufacturing of titanium components is however often challenging. High-speed machining of titanium alloys are particularly challenging. The machining process (metal cutting) induces large plastic deformations and high temperatures, which induce surface integrity changes in the workpiece. This process may affect the material properties and residual stress state of the workpiece at the surface or near surface. The increased speed of cutting as found in high-speed machining may result in significant generation of residual stresses. This is further exacerbated by the low thermal conductivity, high temperature toughness as well as the high chemical reactivity of titanium in general.

The residual stress state of a machined surface is usually evaluated experimentally. This is challenging and expensive and usually involves a non-contact probing technique such as the x-ray diffraction technique. Recently, the semi-destructive fine incremental hole-drilling technique has also been utilised to measure machining-induced residual stresses [1]. Analysis and simulation of the cutting process may therefore significantly reduce the effort to quantify the residual stress state of a machined surface. Recently, Ozel et al [2] showed that "useful" results could be achieved by finite element modelling of the residual stress state and comparison to experimental data. They also concluded that the residual stress state is influenced by the tool micro-geometry. The current work, as reported on in this paper evaluates the effect of constitutive modelling on the residual stress depth profile by comparing orthogonally numerically predicted residual stress state data with X-ray Diffraction (XRD) and synchrotron sourced experimental data [3].

doi:10.1016/j.procir.2014.04.050

2. Material behavior of titanium alloy

At room temperature, titanium (an allotropic element) has hexagonal close packed (hcp) crystalline structure known as (alpha) α-Ti but forms a body centered cubic (bcc) crystalline structure around 900 °C known as (Beta) β-Ti. Typically, 6 % of Aluminium and 4 % vanadium are used as phase stabilizers to obtain an α+β alloy phase [4].During the machining of titanium alloys, it has been found that plastic instability and adiabatic shearing chip serration occurs. Workpiece materials often under goes secondary shearing after the primary shearing zone and a saw-tooth shape chip segment forms [5]. The underlying cause of chip serration is often associated with adiabatic shear formation [6].

The different constitutive models evaluated are: the original Johnson-Cook (material model 1), modified Johnson-Cook with (material model 2) and without (material model 3) temperature dependent flow softening behaviour.

2.1. Material model 1

The original Johnson-Cook (J-C) visco-plastic material model developed to represent material behaviour due to large strains, high strain rates as well as high temperatures [7] is used for material model 1:

$$\sigma = [A + B\varepsilon^n]\left[1 + C\,ln\frac{\dot{\varepsilon}}{\dot{\varepsilon_o}}\right]\left[1 - \left(\frac{T-T_r}{T_m-T_r}\right)^m\right] \quad (1)$$

The J-C material model constants as used by Calamaz et al. [8] were utilised and are presented in Table 1:

Table 1. J-C material model coefficients for Ti6Al4V

Johnson-Cook Model Constants	
A (MPa)	968
B (MPa)	380
n	0.421
C	0.0197
m	0.577
Room Temperature (°C)	25
Melting Temperature (°C)	1 604

Fig. 1 shows flow stress-strain curves versus temperature and strain rates for the *Material Model 1*.

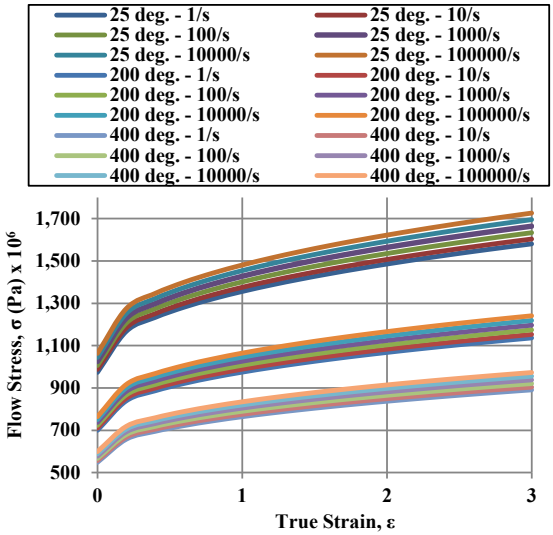

Fig. 1. Flow stress-strain curves versus temperature and strain rate for Material Model1.

2.2. Material model 2

Recent investigations have considered the effects of flow softening and the adiabatic shearing effect on the behaviour of titanium Ti6Al4V alloy at high strains [8]. The flow softening effect is thought to be related to dynamic recovery and/or recrystallisation occurring after a critical value of strain has been reached. The influence of flow softening is more pronounced at low temperatures and as temperatures increase, both strain-hardening and flow softening effects are reduced. Calamaz et al. [8] modified the J-C dynamic material constitutive material model, by multiplying it with a function in order to include flow softening due to higher plastic strain and temperature in their simulations. They were able to simulate serrated chip formation resembling experimental chips.

Sima et al. [5] introduced the exponent S to allow further control of the *tanh* function for the thermal softening in the modified J-C material model.

Eq. 2, 3 and 4 presents the Modified J-C material model as used in the *Material Model 2* simulation.

$$\sigma = \left[A + B\varepsilon^n\left(\frac{1}{exp(\varepsilon^a)}\right)\right]\left[1 + C\ln\frac{\dot{\varepsilon}}{\dot{\varepsilon_o}}\right]\left[1 - \left(\frac{T-T_r}{T_m-T_r}\right)^m\right]\left[D - (1-D)\left[\tanh\frac{1}{(\varepsilon+p)^r}\right]^s\right] \quad (2)$$

$$D = 1 - \left(\frac{T}{T_m}\right)^d \quad (3)$$

$$p = \left(\frac{T}{T_m}\right)^b \quad (4)$$

The Original and Modified J-C material model constants as used by Sima et al. [5] were utilised for

Material Model 2 as shown in Table 2:

Table 2. Modified J-C material model cefficients for Ti6Al4V

Johnson-Cook Model Constants	
A (MPa)	724.7
B (MPa)	683.1
n	0.47
C	0.035
m	1
Room Temperature (°C)	25
Melting Temperature (°C)	1 604
a	2
b	1
d	0.5
r	2
s	5

Fig. 2 shows flow stress-strain curves versus temperature and strain rates for the *Material Model 2*.

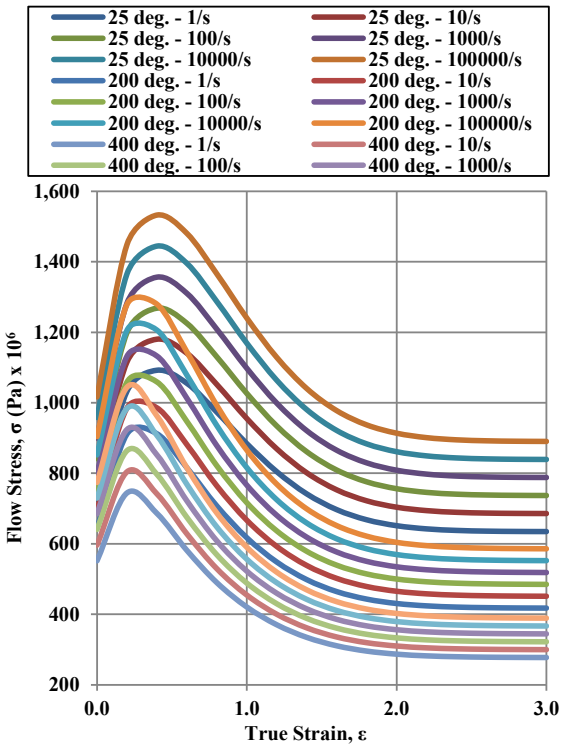

Fig. 2. Flow stress-strain curves versus temperature and strain rate for Material Model 2.

2.3. Material model 3

Essentially the same as equation 2-4 except that the dependent flow softening behaviour is removed. This then becomes:

$$\sigma = [A + B\varepsilon^n]\left[1 + C\ln\frac{\dot{\varepsilon}}{\dot{\varepsilon_o}}\right]\left[1 - \left(\frac{T-T_r}{T_m-T_r}\right)^m\right]\left[M + (1-M)\left[\tanh\frac{1}{(\varepsilon+p)^r}\right]^s\right] \quad (5)$$

The Modified J-C material model constants as used by Ulutan et al. [9] were utilised for *Material Model 3* (Table 3):

Table 3. Modified J-C material model coefficients for Ti6Al4V

Johnson-Cook Model Constants	
A (MPa)	1 000
B (MPa)	625
n	0.55
C	0.029
m	0.995
M	0.48
Room Temperature (°C)	25
Melting Temperature (°C)	1 604
p	0
r	1.2
s	2.7

Fig. 3 shows flow stress-strain curves versus temperature and strain rates for the *Material Model 3*.

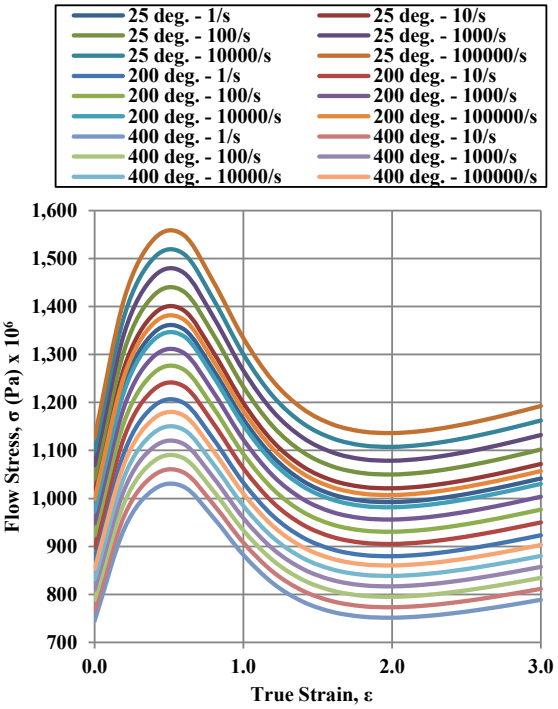

Fig. 3. Flow stress-strain curves versus temperature and strain rate for Material Model 3.

3. Finite element model

A 2D plane strain orthogonal finite element method (FEM) model is set-up to evaluate the chip morphology, tool forces, temperature as well as the machining-induced residual stresses. An implicit coupled analysis was developed to include the heat generated due to plastic work as well as friction. The heat transfer analysis was transient, and the stress analysis ignores inertial effects. A multi-criteria adaptive time stepping procedure was utilised considering a minimum and maximum time step of 1×10^{-10} and 2.5×10^{-3} seconds respectively. This procedure involves the solver initiating a time step size as large as the maximum value set, if the displacement and load convergence tolerances are not met then the time step size is reduced and the procedure is repeated, until convergence is achieved. Fig. 4 shows the set-up of the 2D orthogonal model as used in the simulations.

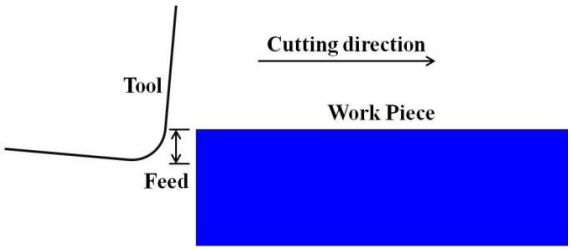

Fig. 4. 2D orthogonal finite element model.

The MSC@ Marc code uses an updated Lagrange re-meshing and solution scheme to overcome severely distorted elements during large plastic deformation. The remeshing was conducted with a minimum mesh size of 5×10^{-7}m. A mesh sensitivity study was conducted considering the appropriate mesh density for prediction of the chip morphology as well as the temperature profile and residual stresses thus predicted. This study also considered analysis time as part of the criteria for selection of the appropriate mesh density. The study determined the best compromise of a denser mesh around the cutting edge in order to capture the adiabatic shear band formation during the machining process. This denser mesh around the cutting edge was then maintained once the tool had been removed and ambient temperature achieved, in order to predict the residual stresses developed by the process. Fig. 5 shows the denser mesh around the cutting edge.

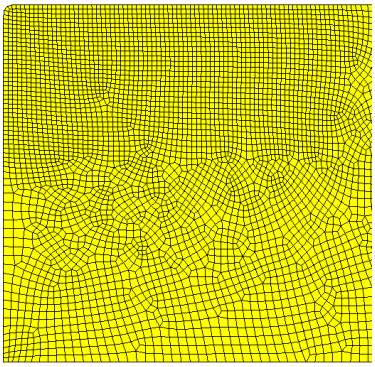

Fig. 5. Denser mesh around the cutting edge.

A feed of 0.2 mm/rev and depth of cut of 1 mm (plane strain thickness), with a cutting speed of 70 m/min was utilised in this work. A cut length of 1 mm was typically modelled. A room temperature of 25 °C (Tr) was assigned to the workpiece. A rigid tool was assumed (no mechanical deformation) with ambient temperature assigned. Heat transfer into the tool from the workpiece due to contact, is considered via a high value for the heat transfer coefficient of 20 000 W/m^2°C [8]. The basic model geometry was selected for direct comparison to available literature. A cutting edge radius of 0.05 mm was modelled along with a rake and relief angle of 5 degrees for both.

The thermal conductivity considered in the analysis was varied linearly as a function of temperature between 20 °C (6.6 W/m°C) and 1 050 °C (21.5 W/m°C). The heat capacity was also varied linearly as a function of temperature between 20 °C (565 J/kg°C) and 980 °C (1 060 J/kg°C). A material density of 4 430 kg.m^{-3} and a thermal coefficient of expansion of $9.4\text{x}10^{-6}$ at room temperature and $1.07\text{x}10^{-5}$ °C^{-1} at 1 000 °C was used. These were all largely based on data from Calamaz et al. [8].Thermal boundary conditions were assumed with an overall forced convection coefficient of 1 000 W/m^{2}K simulating "flood cooling" condition. Fig. 6 shows the "forced convection" boundary conditions applied to the initial mesh of the workpiece. This attribute was re-written to the boundaries during the remeshing phase, before the analysis was resumed, for each time step.

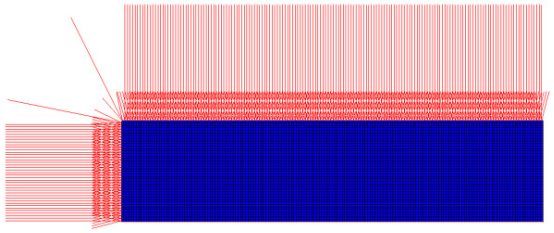

Fig. 6. "Forced convection" boundary conditions applied to simulate "flood cooling" during the process.

The elastic properties of 115 GPa and a Poisson's ratio of 0.3 was derived from Madyira et al [3]. The Coulomb friction law, along with a coefficient of friction of 0.3 was used.

The same model is used with the three different material models is presented.

4. Experimental validation

Experimental data as presented by Madyira et al [3] were used for qualitative comparative purposes. The experimental work consisted of a CNC lathe turning a 75 mm Ti6Al4V (Grade 5) solid round bar at different cutting speeds, feeds as well as depth of cuts, under flood cooled conditions. Only the results for the feed of 0.2 mm/rev, 1 mm depth of cut as well as 70 m/min cutting speed were extracted for this investigation. SANDVIK CNMA 12 04 08 H1P (uncoated carbide) inserts were used throughout. This insert had a negative rake angle of 5°, relief angle of 5°, tool nose radius of 0.8 mm and a cutting edge radius of 0.05 mm. A Kistler, Model 9625B, 3-axis dynamometer along with Type 9441 B Charge Amplifiers and a National Instruments multi-channel data acquisition system were used. This dynamometer was used to measure the three components of the cutting force: F_x – radial force, F_y – tangential and main cutting force and F_z – axial feed force. The experimental set-up is shown in Fig. 7. The parameters of the experimental work is shown in Table 4. The mechanical properties for Ti6Al4V (Grade 5) as per the material certificate are presented in Table 5.

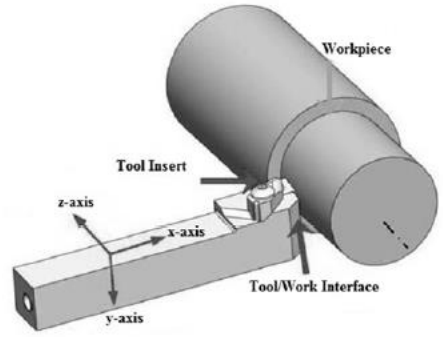

Fig. 7. Experimental set-up.

Table 4. Parameters of the experimental work

Parameter	Condition
Cutting speed (v_c)	70 m/min
Feed rate (f_n)	0.2 mm/rev
Depth of Cut (DOC)	1 mm
Coolant	Flood

Table 5. Material properties for Ti6Al4V (Grade 5)

Ti6Al4V mechanical properties	
Ultimate Tensile Strength (MPa)	1 026.6
0.2% Yield Strength (MPa)	939.3
Young's Modulus (GPa)	115
Elongation (%)	14
Hardness (HRC)	32
Heat Treatment Condition	Annealed

5. Results and discussion

5.1. Cutting force results

The variation of the cutting forces is shown in Fig. 8. The variation of the load for *Material Models 2* and *3* clearly indicates the initial upsetting phase where the workpiece is compressed (cutting force rising rapidly) before the adiabatic shear zone then becomes active and chip segmentation occurs. The cutting force then drops before initiating the next upsetting phase. The maximum experimental cutting force was 429 N. Only the maximum experimentally-determined cutting forces were plotted and not the cyclic forces. The maximum and minimum cutting force for *Material Model 1* was 444 N and 387 N respectively. The maximum and minimum cutting force for *Material Model 2* was 388 N and 176 N respectively. The maximum and minimum cutting force for *Material Model 3* was 504 N and 368 N respectively. The numerically-predicted cutting forces for *Material Models 1* and *2* show good correlations with the experimentally-determined cutting force [10].

The maximum experimental feed cutting force was 205 N. The maximum and minimum cutting force for *Material Model 1* was 282 N and 257 N respectively. The maximum and minimum cutting force for *Material Model 2* was 326 N and 272 N respectively. The maximum and minimum cutting force for *Material Model 3* was 214 N and 178 N respectively. The numerically-predicted feed cutting forces indicate poor comparison with the experimentally-determined cutting force [10]. This could be due to the friction law as well as coefficient of friction chosen in the simulations.

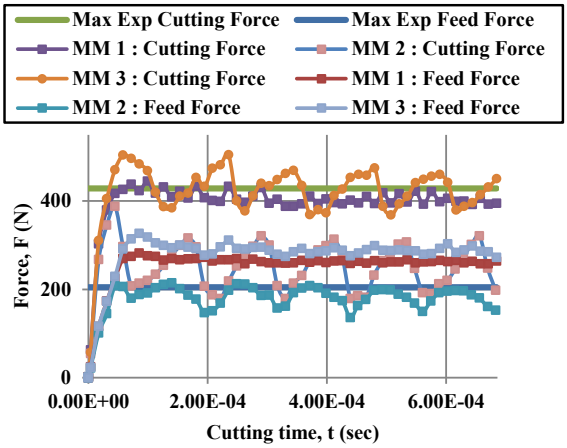

Fig. 8. Variation of the cutting and feed forces to experimental data [10].

5.2. Temperature results

Temperature contour plots also outlining the chip morphology are presented for the different materials models in Figures 9 to 11. Maximum temperatures of 789 °C, 506 °C and 816 °C for *Material Model 1*, *Material Model 2* and *Material Model 3* respectively, is predicted. *Material Model 2* predicted a temperature closest to that presented by Calamaz et al. [8] that determined a maximum workpiece temperature of 570 °C at a cutting speed of 60 m/min. Bowes [11] measured machining temperatures 1 mm from the tool tip cutting edge with the use of fibre optics, during dry orthogonal machining of Ti6Al4V. A maximum machining temperature of 641 °C was measured, based on a depth of cut (width) of 3 mm, feed rate of 0.1 mm/rev at a cutting speed of 75 m/min. *Material Model 1* and *Material Model 3* are higher than these sets of published data. This is most likely due to the excessive strain hardening and insufficient thermal as well as strain softening in these two material models. In addition, different tool and workpiece material properties were however used and the effect of the forced convection boundary condition as used in the current investigation to simulate "flood cooling" is difficult to quantify without substantial additional work. *Material Models 2* and *3* do however correctly predict the onset of the "adiabatic shear band" phenomenon as well as the typical segmented chip morphology typical of titanium machining with material model 2 displaying the best comparison with morphology data as published by Calamaz [8] .

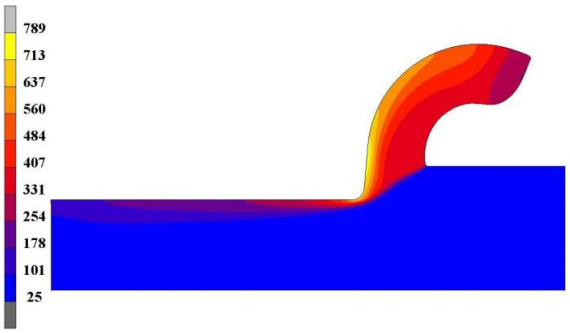

Fig. 9. Temperature distribution in the workpiece for Material Model 1.

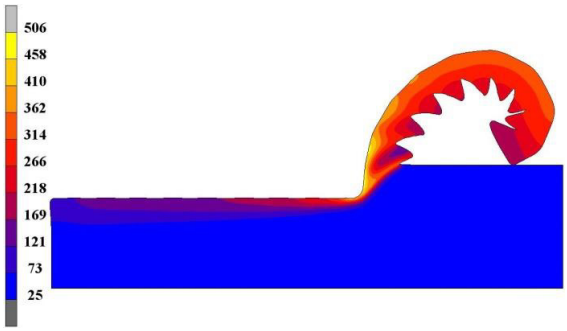

Fig. 10. Temperature distribution in the workpiece for Material Model 2.

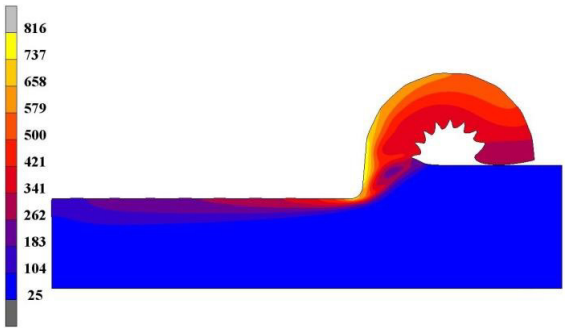

Fig. 11. Temperature distribution in the workpiece for Material Model 3.

5.3. Machining-induced residual stress results

The machining-induced residual stresses are determined upon removal of the tool and the return of the workpiece to room temperature along with removal of the "chip" to allow for any possible "spring-back" that may occur. The stresses were measured at the center of the length of cut, through the thickness of the workpiece.

Fig. 12 presents a comparison of the residual stress field for the different material models as a function of depth. *Material Model 2* and the experimental results indicate compressive residual stresses at and near the machined surface, becoming tensile before reaching the

unstressed parent material. This is typical of residual stress profiles when machining titanium. The residual stress profiles differ greatly through the thickness of the workpiece. The experimental data reveals a compressive residual stress of 402 MPa at a depth of 15 µm whereas the results for *Material Model 2* predict a compressive residual stress of 27 MPa at this same depth. The results for *Material Model 1* predict a tensile residual stress of 11 MPa at 15 µm and *Material Model 3* a tensile residual stress of 136 MPa.

Clearly the depth profiles obtained for the different materials models show significant differences when compared to one another and when compared to literature experimental data. There can be various reasons for this including the fact that the comparative experimental data was for conventional outside turning and therefore not fully orthogonal. This will have an effect on the effective chip thickness (feed rate) when compared to an orthogonal process but in general residual stress field near surface for titanium alloys has been demonstrated to be mostly fully compressive. Model 2 correctly predicts a compressive residual stress albeit smaller than the literature data suggests. A compressive residual stress field is largely a function of the heat generated and the subsequent distribution of such in the tool, chip and workpiece.

The material models evaluated in this study indicate the influence of the plastic heat generated due to the extent of the strain hardening of the particular model, and hence the temperature thus generated. This in turn has an effect on the thermal and strain softening that occurs during the process.

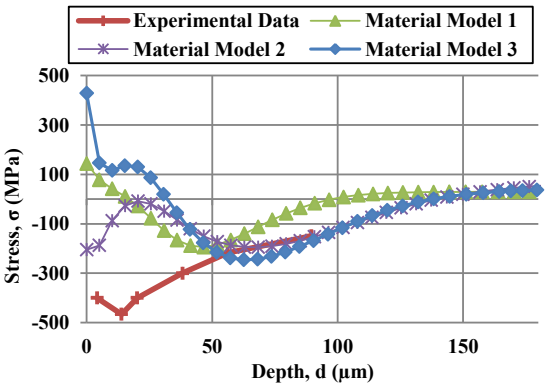

Fig. 12. Numerically determined residual stress depth profile as compared to experimental data [3].

Conclusion

This paper describes a finite element evaluation of the effect of different constitutive models on machining induced residual stresses for Ti6Al4V titanium alloy.

The cutting forces for *Material Model 1* and *2* indicate the fluctuation in load due to the development of a shear band after the upsetting stage of serrated chip generation. The peak cutting forces predicted for *Material Model 2* are lower than the experimental results. This is due to the additional flow softening occurring due to temperature dependence. *Material Models 1* and *2* show good correlation with published data.

Material Model 2 predicted a maximum temperature closest to the published data. *Material Models 1* and *3* indicate higher temperatures that would be due to excessive strain hardening as well as inadequate flow softening at the appropriate strain levels.

The prediction of the machining-induced residual stress indicated significant differences in the results, both at and near the machined surface. *Material Models 1* and *3* predicated tensile residual stresses at the surface of the workpiece. As stated previously this could be due to increased strain hardening and insufficient flow softening. *Material Model 2* predicted compressive residual stress at the machined surface as typically found when machining titanium. The numerically-predicted feed cutting forces indicate poor comparison with the experimentally-determined cutting force. This could be due to the friction law as well as coefficient of friction chosen in the simulations.

Essentially this investigation has shown that numerical modelling as a tool has reached a point where most material and kinematic behaviour as regards to orthogonal machining can be modelled in good agreement with individual experimental data depending on what the specific criteria of assessment is. A comprehensive constitutive model coupled to a kinematic model that adequately describes all aspects of the cutting process including chip morphology, cutting forces, and the residual stress field as a function of the various appropriate cutting parameters has yet to be demonstrated especially for titanium alloys. One of the main reasons for this is the relative shortage of extensive and reliable experimental data applicable to a specific set of cutting parameters.

References

[1] P. Grant, J. Lord, P. Whitehead and T. Fry, "The applicaton of fine increment hole drilling for measuring machining-induced residual stresses," *Applied Mechanics and Materials,* Vols. 3-4, pp. 105-110, 25 March 2005.

[2] T. Ozel and D. Ulutan, "Predicition of machining induced residual stresses in turning of titanium and

nickel based alloys with experiments and finite element simulations," *CIRP Annals - Manufacturing Technology,* vol. 61, pp. 547-550, 2012.

[3] D. Madyira, R. F. Laubscher, N. Janse van Rensburg and P. F. Henning, "High speed machining induced residual stresses in Grade 5 titanium alloy," *Proceedings of the Institution of Mechanical Engineers, Part L : Journal of Materials Design and Applications,* vol. 227, no. 3, pp. 208-215, 2013.

[4] S. Nemat-Nasser and J. B. Isaacs, "Direct measurement of isothermal flow stress of metals at elevated temperatures and high strain rates with application to Ta and Ta–W alloys," *Acta Materialia,* vol. 45, pp. 907-919, 1997.

[5] M. Sima and T. Ozel, "Modified material constitutive models for serrated chip formation simulations and experimental validation in machining of titanium alloy Ti-6Al-4V," *International Journal of Machine Tools & Manufacture,* vol. 50, pp. 943-960, 2010.

[6] R. Komanduri and Z. B. Hou, "On thermoplastic shear instability in the machining of a titanium alloy," *Metallurgical and Materials Transactions,* vol. A33A, pp. 2995-3010, 2002.

[7] G. R. Johnson and W. H. Cook, "A constitutive model and data for metals subjected to large strains, high strain rates and high temperatures," in *Proceedings of the 7th International Symposium on Ballistics, Vol. 21 : International Ballistics Commitee*, The Hague, Netherlands, 1983.

[8] M. Calamaz, D. Coupard and F. Girot, "A new material model for 2D numerical simulation of serrated chip formation when machining titanium alloy Ti–6Al–4V," *International Journal of Machine Tools & Manufacture,* no. 48, pp. 275 - 288, 2008.

[9] D. Ulutan and T. Ozel, "Determination of tool friction in presence of flank wear and stress distribution based validation using finite element simulations in machining of titanium and nickel based alloys," *Journal of Materials Processing Technology,* vol. 213, no. 12, pp. 2217-2237, 2013.

[10] K. D. Edkins, An investigation of machining induced residual stresses on Grade 4 and 5 titanium alloys, Johannesburg: University of Johannesburg, 2012.

[11] D. C. Bowes, Numerical Modelling of Ti6Al4V Machining: A Combined FEA and Unified Mechanics of Cutting Approach, Stellenbosch: Stellenbosch University, 2013.